RSC Advances

PAPER

View Article Online
View Journal | View Issue

Cite this: *RSC Adv.*, 2017, **7**, 36860

Construction of 3D metal–organic frameworks bearing heteropolyoxometalate units and multi-azole molecules and exploration of their photocatalytic activities†

Chunhua Gong,[ab] Xianghua Zeng,[a] Li Xin,[a] Junyong Zhang*[a] and Jingli Xie[a]

Taking advantage of multi-azole molecules as organic linkers, two novel 3D metal–organic frameworks consisting of heteropolyoxometalate building blocks, *i.e.*, $[Cu_5(1,4\text{-ttb})_4(CrMo_6(OH)_6O_{18})(H_2O)_8]\cdot 10H_2O$ (**1**) and $[Cu_4(1,4\text{-ttb})_4(SiW_{12}O_{40})(H_2O)_8]\cdot 4H_2O$ (**2**) (1,4-ttb = 1-(tetrazo-5-yl)-4-(triazo-1-yl)benzene) have been fabricated and characterized *via* X-ray single-crystal diffraction, FT-IR spectroscopy, powder X-ray diffraction (PXRD) and TG analyses. Compounds **1** and **2** both possess pillared-layer 3D frameworks which were based on POM units and different Cu–tetrazolate motifs. Compound **1** is a (2,6,6)-connected 3D framework constructed from the 2D networks $\{Cu_5(1,4\text{-ttb})_4(H_2O)_8\}_n$ through connected $CrMo_6$ polyoxoanions with $(3^2.4^2.5^2.6^8.8)(3^4.4^4.5^4.6^3)$ topology. Compound **2** is a (2,3,5)-connected 3D framework constructed from the 2D wave layers $\{Cu_4(1,4\text{-ttb})_4(H_2O)_8\}$ through connected SiW_{12} polyoxoanions with $(4.8^2)_2(4^2.6^4.8^2.10^2)(8)$ topology. Magnetism studies of compound **1** reveal the dominant antiferromagnetic coupling between the Cu(II) ions. The electrochemistry properties of compound **2** were studied. Intriguingly, compounds **1** and **2** display considerable photocatalytic activities for the degradation of several organic dyes.

Received 9th May 2017
Accepted 19th July 2017

DOI: 10.1039/c7ra05210c

rsc.li/rsc-advances

Introduction

Polyoxometalates (POMs) have attracted overwhelming interest because of the richness of structural characters and potential applications in catalysis, photochemistry and electrochemistry.[1] As basic inorganic oxygen-cluster units, POMs have large amounts of terminal O atoms (O_t) and bridging O atoms (O_b), and could act as building blocks to construct fascinating metal–organic frameworks (MOFs) with new functional properties.[2] By introducing the rigid ligands to serve as bridging units, namely organic ligands combine with inorganic oxygen-cluster units, it is anticipated that significantly POM-based framework materials could be achieved due to the variety of coordination sites of this type of ligand. In this regard, the selection of bridging ligands is still the key factor in the effective synthesis of POM-based MOFs. Multi-azole organic molecules with more adjacent coordination sites, such as triazole and tetrazole derivatives, can link metal ions and promote the formation of multinuclear metal clusters, and the generation of multinuclear metal clusters may also endow compounds a number of significant intrinsic properties such as magnetic properties and multifunctional properties. Among them, 1-(tetrazo-5-yl)-4-(triazo-1-yl)benzene (1,4-ttb) has been exploited to construct a series of metal–organic coordination compounds.[3] However, to the best of our knowledge, the combination of this type of rigid ligand and POMs units remains scarce. Peng's group has obtained some particularly interesting POMs-based MOFs by using the rigid 5-(4-imidazol-1-yl-phenyl)-2*H*-tetrazole as linkers, and they studied the fluorescence and electrochemical properties of the compounds.[4] Sun's group used rigid ligands such as 5′-(pyridin-2-yl)-1*H*,2′*H*-3,3′-bi(1,2,4-triazole), 1-(tetrazo-5-yl)-4-(triazo-1-yl)benzene and 3,3′,5,5′-tetramethyl-4,4-bipyrazole and synthesized four Preyssler P_5W_{30}-based MOFs, and the magnetism property, electrocatalytic abilities toward the reduction of hydrogen peroxide and the catalytic activities in the cyanosilylation of aldehydes reaction were investigated.[5] These results have demonstrated the potential of constructing POMs-based MOFs by virtue of 1,4-ttb ligand, and exploring the diversity of structural characters of POMs under different experimental conditions, and furthermore, enabling the formation of a series of promising functional materials.

Herein we reported two novel copper-based compounds with 1,4-ttb ligand and different hetero-POMs, namely, $[Cu_5(1,4\text{-ttb})_4(CrMo_6(OH)_6O_{18})(H_2O)_8]\cdot 10H_2O$ (**1**) and

[a]*College of Biological, Chemical Science and Engineering, Jiaxing University, Jiaxing 314001, P. R. China. E-mail: zhangjy@mail.zjxu.edu.cn*

[b]*State Key Laboratory of Structural Chemistry, Fujian Institute of Research on the Structure of Matter, Chinese Academy of Sciences, Fuzhou 350002, P. R. China*

† Electronic supplementary information (ESI) available: Table of selected bond lengths and angles, IR, PXRD, TG, and additional figures. CCDC 1497463 and 1497464. For ESI and crystallographic data in CIF or other electronic format see DOI: 10.1039/c7ra05210c

$[Cu_4(1,4\text{-ttb})_4(SiW_{12}O_{40})(H_2O)_8]\cdot 4H_2O$ (**2**). Those two compounds both display POM-based pillared-layer 3D frameworks modified by different Cu–tetrazolate motifs. Compound **1** is a (2,6,6)-connected 3D framework constructed from the 2D networks $\{Cu_5(1,4\text{-ttb})_4(H_2O)_8\}_n$ through connected $CrMo_6$ polyoxoanions with $(3^2.4^2.5^2.6^8.8)(3^4.4^4.5^4.6^3)$ topology. Compound **2** is a (2,3,5)-connected 3D framework constructed from the 2D wave layers $\{Cu_4(1,4\text{-ttb})_4(H_2O)_8\}$ through connected SiW_{12} polyoxoanions with $(4.8^2)_2(4^2.6^4.8^2.10^2)(8)$ topology. The magnetic property of compound **1** and the electrochemistry property of compound **2** were explored. In addition, in the aqueous solution of three organic dyes, the photodegradation effect of **1** and **2** were investigated, and intriguingly, they display considerable photocatalytic activities.

Experimental

Materials and general methods

All the chemicals were received as reagent grade and used without any further purification. $Na_3[CrMo_6(OH)_6O_{18}]\cdot 8H_2O$ were synthesized according to literatures.[6] The IR spectra were obtained on a Varian 640 FT-IR spectrometer with KBr pellet in 400–4000 cm^{-1} region. Powder X-ray diffraction (PXRD) was performed on a DX-2600 spectrometer. The thermal gravimetric analyses (TGA) were carried out in flowing N_2 on a SDT 2960 differential thermal analyzer with a rate of 10 °C min^{-1}. Variable-temperature direct current (DC) magnetic susceptibility data down to 2 K on microcrystalline samples were carried out on a Quantum Design MPMP-XL7 superconducting quantum interference device (SQUID) magnetometer equipped with a 7 T DC magnet. Cyclic voltammograms were obtained with a CHI 440A electrochemical workstation at room temperature. Platinum wire was used as a counter electrode and Ag/AgCl electrode was as a reference electrode. Chemically bulk-modified carbon paste electrode (CPE) was used as the working electrode. The UV experiments were carried out on a Thermo EV 201CP.

Synthesis of $[Cu_5(1,4\text{-ttb})_4(CrMo_6(OH)_6O_{18})(H_2O)_8]\cdot 10H_2O$ (1). A mixture of $Na_3[CrMo_6(OH)_6O_{18}]\cdot 8H_2O$ (120 mg, 0.1 mmol), $Cu(NO_3)_2\cdot 3H_2O$ (120 mg, 0.5 mmol), 1,4-ttb (23 mg, 0.1 mmol), DABCO (13 mg, 0.1 mmol) and 10 mL water was stirred for 1 h. The pH of the solution was adjusted to 2.5 with HCl (4 mol L^{-1}). The resulting solution was transferred to a Teflon-lined reactor and kept under autogenous pressure at 160 °C for 3 days. After slow cooling to room temperature, blue block crystals of **1** were filtered, washed with distilled water and dried at room temperature (yield, 45%, based on Cu). Anal. calcd for $C_{36}H_{30}N_{28}O_{31}Cu_5CrMo_6$ (2296.22): C 18.83, H 1.32, N 17.08; found: C 19.01, H 1.25, N 16.85. IR (solid KBr pellet, cm^{-1}): 3397(s), 3118(s), 1609(s), 1521(s), 1469(s), 1283(w), 1215(w), 1159(s), 947(m), 916(s), 839(s), 643(s), 562(w).

Notably, the successful synthesis of **1**, rely on the finding that the addition of 1,4-diazabicyclo[2.2.2]octane (DABCO) can affect the synthetic process. Although the DABCO is not involved into the final product, it may play the role as the template during the reaction process which are supported by several initial experiments: (1) in absence of DABCO, no crystalline materials of **1** could be observed; (2) decrease the amount of DABCO to one-quarter or one-half of the original value only lead to very few tiny crystalline **1**.

Synthesis of $[Cu_4(1,4\text{-ttb})_4(SiW_{12}O_{40})(H_2O)_8]\cdot 4H_2O$ (2). A mixture of α-$K_8SiW_{11}O_{39}\cdot 13H_2O$ (140 mg, 0.1 mmol), $Cu(NO_3)_2\cdot 3H_2O$ (120 mg, 0.5 mmol), 1,4-ttb (23 mg, 0.1 mmol) and 10 mL water was stirred for 1 h. The pH of the solution was adjusted to 2.5 with 4 mol L^{-1} HCl. The resulting solution was transferred to a Teflon-lined reactor and kept under autogenous pressure at 160 °C for 3 days. After slow cooling to room temperature, blue block crystals of **2** were filtered, washed with distilled water and dried at room temperature (yield, 35%, based on Cu). Anal. calcd for $C_{36}H_{48}N_{28}O_{52}Cu_4SiW_{12}$ (4193.47): C 10.31, H 1.15, N 9.35; found: C 10.38, H 1.10, N 9.28. IR (solid KBr pellet, cm^{-1}): 3387(s), 3154(s), 1689(s), 1543(s), 1477(s), 1262(w), 1204(w), 1196(s), 967(m), 921(s), 842(s), 651(s), 564(w).

Preparation of compound 2-CPE. The preparation method is as follows:[7] a mixture of 100 mg graphite powder and 10 mg target compound was grinded in an agate mortar for approximately 30 minutes to achieve a uniform mixture. Then one drop methylsilicone oil was added and stirred into paste with a copper rod. The paste mixture was packed into a 2 mm inner diameter glass tube and the tube surface was rubbed into smooth on a weighing paper. The electrical contact was established with the copper rod through the back of the electrode. The bare CPE was prepared by similar process without target compound.

X-ray crystallographic study

X-ray diffraction analysis data for compounds **1–2** were collected with an Oxford Diffraction Gemini R Ultra

Table 1 Crystal data and structure refinements for compounds **1** and **2**[a,b]

	Compound **1**	Compound **2**
Empirical formula	$C_{36}H_{30}N_{28}O_{31}Cu_5CrMo_6$	$C_{36}H_{48}N_{28}O_{52}Cu_4SiW_{12}$
Formula weight	2296.22	4193.47
Crystal system	Triclinic	Monoclinic
Space group	$P\bar{1}$	$P2_1/n$
a (Å)	12.8771(6)	10.8478(3)
b (Å)	13.4775(6)	13.1152(3)
c (Å)	13.5993(5)	27.6434(6)
α (°)	107.916(4)	90.00
β (°)	103.921(3)	98.886(2)
γ (°)	112.783(4)	90.00
V (Å^3)	1888.46(15)	3885.65(16)
Z	1	2
D_c (g cm^{-3})	2.019	3.584
μ (mm^{-1})	2.567	18.886
F (000)	1111.0	3788.0
Reflections collected	13 711	17 362
Independent reflections	6634	6846
R_{int}	0.0179	0.0266
GOOF	1.060	1.050
R_1, wR_2[I ≥ 2σ(I)]	0.0317, 0.0813	0.0868, 0.1857
R_1, wR_2[all data]	0.0367, 0.0841	0.0903, 0.1870

[a] $R_1 = \Sigma||F_o| - |F_c||/\Sigma|F_o|$. [b] $wR_2 = \Sigma[w(F_o^2 - F_c^2)^2]/\Sigma[w(F_o^2)^2]^{1/2}$.

diffractometer with graphite-monochromated Mo-Kα (λ = 0.71073 Å) at 296 K. All structures were solved by direct methods and refined on F^2 by full-matrix least-squares methods using the SHELXTL package.[8] In the structure of compound **1**, the solvate water molecules are heavily disordered over multiple positions, and this electron density was modeled using a squeeze routine implemented in PLATON.[9] A summary of the crystal data and structure refinements of compounds **1–2** are provided in Table 1. Selected bond lengths and angles are listed in Table S1 in the ESI.† Crystallographic data for compounds **1–2** have been deposited in the Cambridge Crystallographic Data Center, their crystal structures can be obtained with CCDC reference numbers 1497463 and 1497464, respectively.

Results and discussion

Description of the crystal structures

$[Cu_5(1,4\text{-ttb})_4(CrMo_6(OH)_6O_{18})(H_2O)_8]\cdot 10H_2O$ (1). X-ray single crystal diffraction analysis reveals that compound **1** is obtained as a Anderson type $CrMo_6$ anion pillared-layer 3D framework incorporating 2D $[Cu_5(1,4\text{-ttb})(H_2O)_8]$ sheets. Compound **1** crystallizes in the triclinic space group $P\bar{1}$, and the crystal structure consists of one $[CrMo_6(OH)_6O_{18}]^{3-}$ (abbreviated as $CrMo_6$) polyoxoanion, four 1,4-ttb ligands, five copper ions, eight coordination water molecules and ten crystallization water molecules. Bond valence sum calculations[10] show that all molybdenum atoms are in the +6 oxidation state, and copper atoms are in the +2 oxidation state.

As shown in Fig. 1, there are three crystallographically independent Cu ions with two kinds of coordination modes in the structure of compound **1**. Cu1 ion is six-coordinated in a octahedral geometry by two O atoms from two $CrMo_6$ polyoxoanions and four N atoms from 1,4-ttb ligands. Similarly, Cu2 ion is six-coordinated in a distorted octahedral geometry by two N atoms from two 1,4-ttb ligands and four O atoms from water molecules. While Cu3 ion is five-coordinated by three N atoms from two tetraazole and a trizole in three different 1,4-ttb ligands and two O atoms from two water molecules to form a square pyramidal geometry. The bond lengths ranges of Cu–O and Cu–N are 1.915(3)–2.307(3) Å and 1.955(3)–2.137(5) Å, respectively (Table S1†).

In **1**, four Cu ions (two Cu2, two Cu3 ions) are aggregated by tetrazolyl groups, forming a tetra-nuclear subunit. The tetra-nuclear subunits are linked together *via* 1,4-ttb ligands, forming an infinite $\{Cu_4(1,4\text{-ttb})_4\}_n$ chains (Fig. 2a). Furthermore, these chains are bridged *via* Cu1 ions coordinated by two N atoms from the remaining triazole groups from adjacent chains to form an interesting 2D network $\{Cu_5(1,4\text{-ttb})_4\}_n$ (Fig. 2b).

The 3D framework structure of compound **1** is constructed from the 2D networks through covalently connected $CrMo_6$ polyoxoanion (Fig. 3a). Each $CrMo_6$ polyoxoanion from a framework offers two terminal oxygen atoms to coordinate to Cu1 ions from neighboring networks. Considering $\{Cu_4(1,4\text{-ttb})_4\}_n$ chain and Cu1 ion as six-connected nodes, the $CrMo_6$ polyoxoanion as two-connected nodes, as a result, compound **1** is a (2,6,6)-connected 3D framework with $(3^2.4^2.5^2.6^8.8)(3^4.4^4.5^4.6^3)$ topology (Fig. 3b).

$[Cu_4(1,4\text{-ttb})_4(SiW_{12}O_{40})(H_2O)_8]\cdot 4H_2O$ (2). X-ray single crystal diffraction analysis reveals that compound **2** is obtained as a Keggin type SiW_{12} anion pillared-layer 3D framework incorporating 2D $[Cu_4(1,4\text{-ttb})_4(H_2O)_8]$ sheets. Compound **2** consist of one $[SiW_{12}O_{40}]^{4-}$ (abbreviated as SiW_{12}) polyoxoanion, four 1,4-ttb ligands, four Cu ions, eight coordinated water molecules and four crystallization water molecules. Bond valence sum calculations[10] show that all tungsten atoms are in the +6 oxidation state, and copper atoms are in the +2 oxidation state.

In compound **2**, there are two crystallographically independent Cu ions (Fig. 4). Cu1 is coordinated by four N atoms from four 1,4-ttb ligands, one O atom from one SiW_{12} polyoxoanion and one O atom from water molecule. Cu2 is five-coordinated by two N atoms from two 1,4-ttb ligands and three O atoms from three water molecules. The corresponding bond lengths ranges of Cu–O and Cu–N are 1.95(3)–2.367(18) Å and 1.96(2)–2.10(2) Å, respectively (Table S1†).

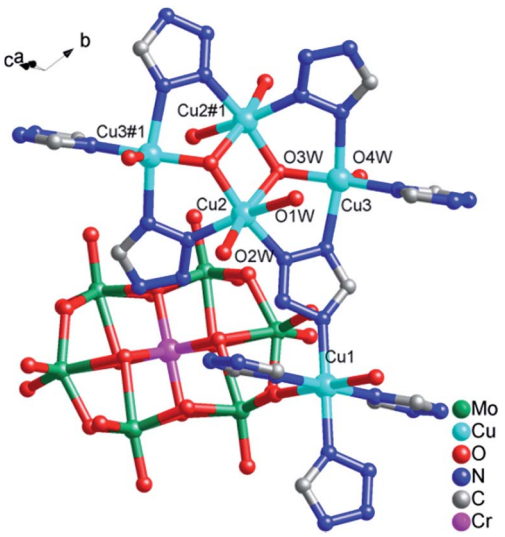

Fig. 1 The coordination modes of Cu ions in compound **1**. The hydrogen atoms are omitted for clarity. Symmetry codes: #1 1 − *x*, 2 − *y*, −*z*.

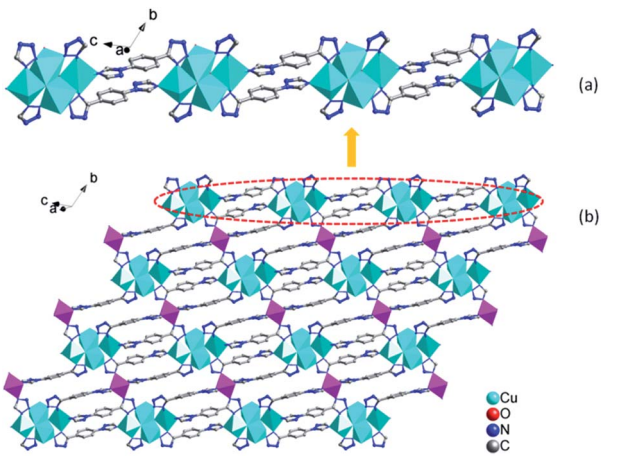

Fig. 2 (a) View of the 1D $\{Cu_4(1,4\text{-ttb})_4\}_n$ chains. (b) View of the 2D network.

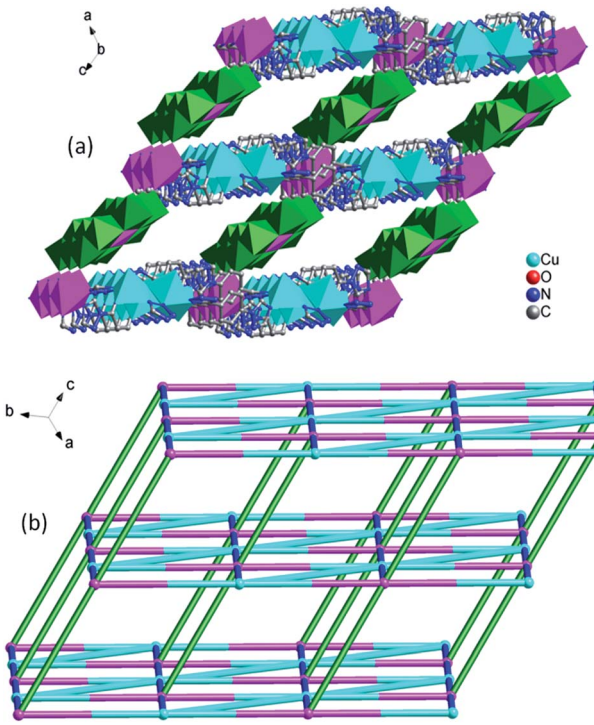

Fig. 3 (a) View of the 3D structure of compound **1**. The hydrogen atoms are omitted for clarity. (b) Schematic view of the 3D framework structure of compound **1**. The light blue, pink, green and blue nodes represents the $\{Cu_4(1,4\text{-ttb})_4\}_n$ chain, Cu1 ions, $CrMo_6$ polyoxoanion and 1,4-ttb ligands.

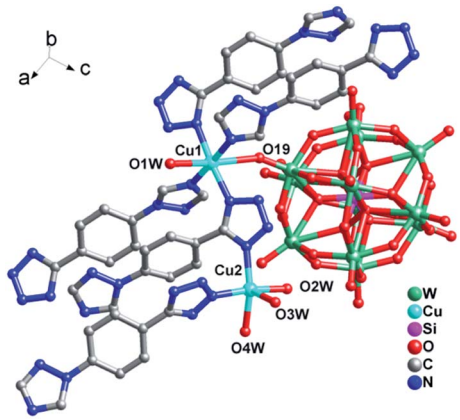

Fig. 4 Ball/stick/polyhedral view of the asymmetric unit of compound **2**. The hydrogen atoms and crystallization water molecule are omitted for clarity.

In compound **2**, the 1D left-hand chain is formed from Cu ions bridged by tetrazolyl groups from 1,4-ttb ligand (Fig. 5a). Furthermore, the chains are connected by the 1,4-ttb ligand to generate a 2D wave layer (Fig. 5b). Finally, each SiW_{12} polyoxoanion offers two O atoms to connect Cu ions from two neighboring layer to extend the layers into a 3D framework structure (Fig. 6a). Considering Cu2 ions as two-connected nodes, the 1,4-ttb ligand as three-connected nodes, the Cu1 ions as five-connected nodes, as a result, compound **2** is a (2,3,5)-connected 3D framework with $(4.8^2)_2(4^2.6^4.8^2.10^2)(8)$ topology (Fig. 6b).

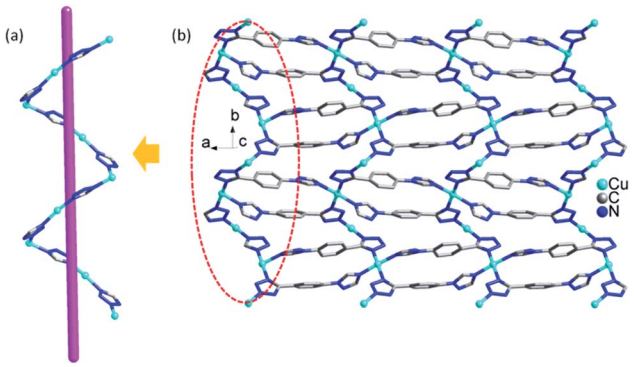

Fig. 5 (a) The 1D chain in compound **2**. (b) The 2D layer of compound **2**.

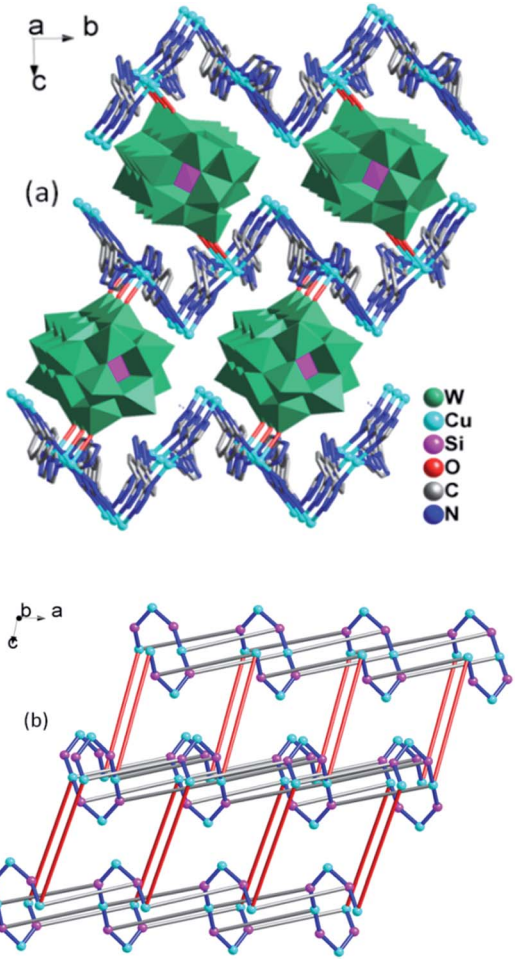

Fig. 6 (a) View of the 3D structure of compound **2**. (b) The light blue, pink, gray and red nodes represents the Cu1 and Cu2 ions, tetrazole, 1,4-ttb ligand and SiW_{12} polyoxoanion.

FT-IR spectra, powder X-ray diffraction (PXRD) and TG analyses

The IR spectra of compound **1** and **2** are shown in Fig. S1.† For compound **1**, the bands at 947, 916, 839, 643 and 562 cm^{-1} could be ascribed to the characteristic peaks of υ_{as} (Mo–O), υ_{as}

(Cr–O), υ_{as} (Mo–O–Mo), υ_{as} (Mo–O–Cr). For compound **2**, the bands at 967, 921, 842, 651 and 564 cm^{-1} could be ascribed to the characteristic peaks of υ_{as} (Si–O), υ_{as} (W–O), υ_{as} (W–O–W). The absorption peaks at 1609–1159 cm^{-1} for **1** and 1689–1196 cm^{-1} for **2** are assigned to the vibrations of C–N, C=C, N=N of 1,4-ttb ligand. In addition, a broad band around 3400 cm^{-1} should be attributed to the vibration of O–H in water molecules.

To testify the phase purities of compound **1** and **2**, PXRD experiments were carried out. As shown in Fig. S2,† the diffraction peaks of both simulated and experimental patterns match well in the key positions, which indicate that the powders of the two compounds are single phase. The intensity differences can be owed to the different orientation of the powder samples.

The thermal stabilities of compounds **1** and **2** were measured in flowing N_2 from room temperature to 800 °C with a heating rate of 10 °C min^{-1}. As shown in Fig. S3,† both curves show two-step weight loss processes. In compound **1**, the first weight loss of 8.51% (calc. 8.62%) occurs before 182 °C, which is attributed to the loss of water molecules. For compound **2**, it starts to lose weight at 173 °C with the weight loss of 3.08% (calc. 3.43%), which is corresponding to the loss of water molecules. The second weight losses of compounds **1** and **2** are ascribed to the decomposition of 1,4-ttb ligands.

Magnetic property of compound 1

The variable-temperature magnetic susceptibility of **1** was measured from 1.8 to 310 K at 2000 Oe, owing to the butterfly trinuclear complex units. As shown in Fig. 7, the $\chi_m T$ value at 300 K was 3.02 emu mol^{-1} K, which was larger than the spin-only value of 1.52 emu mol^{-1} K for the uncorrelated four Cu(II) ($S = 1/2$) with $g = 2.00$. Upon cooling, with decreasing temperature, the $\chi_m T$ value gradually decreases and reaches a minimum value of 1.31 emu mol^{-1} K at 3 K and then slightly increases to 1.36 emu mol^{-1} K at 1.8 K. The $\chi_m T$ *vs.* T plot in the temperature range of 3–300 K indicates dominant antiferromagnetic coupling between the Cu(II) ions.

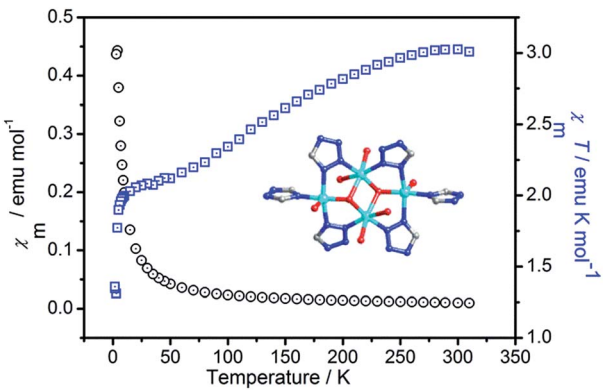

Fig. 7 Temperature-dependent magnetic susceptibility of compound **1** in the temperature range of 2–300 K under an applied field of 2000 Oe.

Electrochemical property of 2-CPE

The electrochemical property of **2**-CPE has been investigated in detail in 0.5 M Na_2SO_4 + 0.1 M H_2SO_4 aqueous solution. In the potential range from −800 to −100 mV, there are three pairs of reversible redox peaks (I–I′, II–II′, III–III′) for compound **2** (Fig. 8a), which could be assigned to the redox process of SiW_{12} anion.[11] The mean peak potentials $E_{1/2} = (E_{cp} + E_{ap})/2$ are −230, −480 and −730 mV, respectively. In addition, when the scan rates vary ranges of 50–500 mV s^{-1}, the peak potentials change gradually: the cathodic peak potentials shift toward the negative direction and the corresponding anodic peak potentials to the positive direction. As shown in Fig. 8b, the peak currents are proportional to the scan rates, which shows that the redox process of **2**-CPE are surface-controlled.[12]

Photocatalytic activity

A wide range of POMs-based MOFs possess photocatalytic activities in the degradations of organic dyes under light

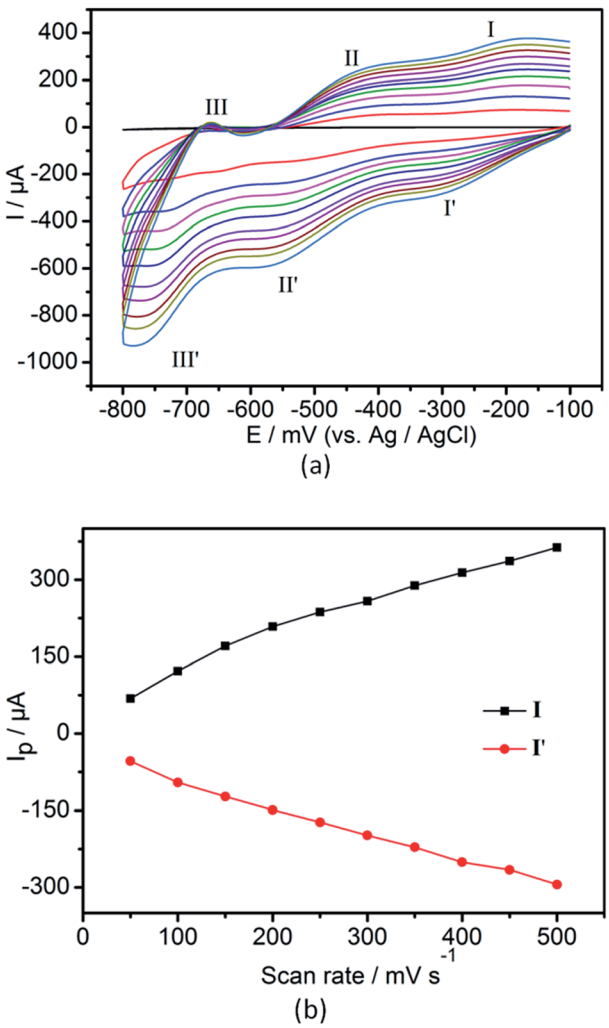

Fig. 8 (a) Cyclic voltammogram of **2**-CPE in 0.5 M Na_2SO_4 + 0.1 M H_2SO_4 aqueous solution. Potentials measured *vs.* Ag/AgCl (from inside to out: 50, 100, 150, 200, 250, 300, 350, 400, 450, 500 mV s^{-1}).

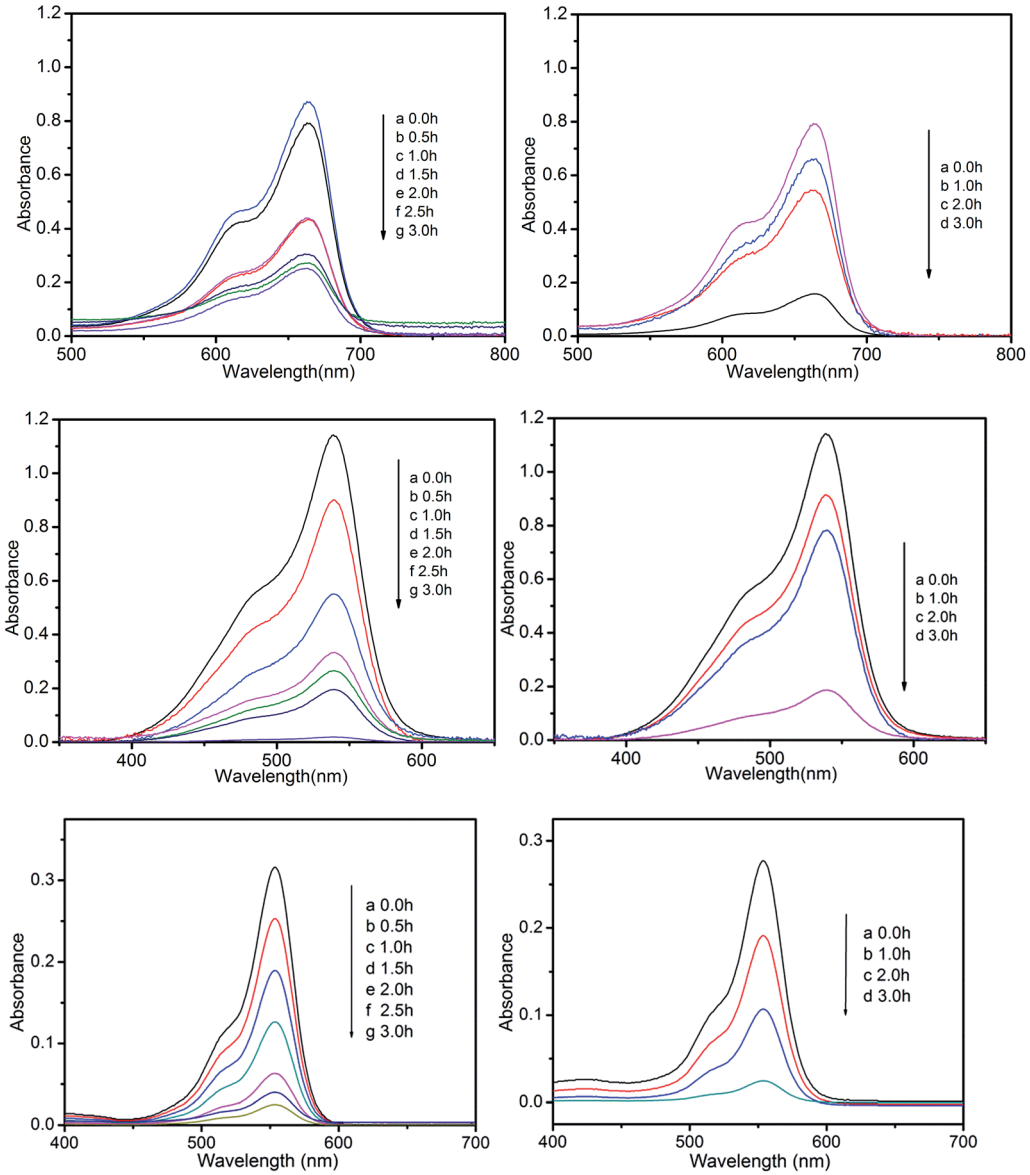

Fig. 9 Photocatalytic decomposition of MB, PH, and RhB solution under UV with the use of compounds **1** (left) and **2** (right).

irradiation.[13] Hence, we also investigated the photocatalytic performance of compounds **1** and **2** for the photodegradation of methylene blue (MB), pararosaniline hydrochloride (PH), and rhodamine B (RhB) with UV irradiation through a typical process: compounds **1** (15 mg) and **2** (15 mg) were respectively added into the 50 mL aqueous solution of MB, Ph, and RhB, then the obtained suspensions were magnetically stirred in the dark for about 15 min to ensure the equilibrium of working solution (for control experiments under the same reaction conditions without any catalyst). The solution was then exposed to UV irradiation from a 100 W Hg lamp (λ = 365 nm). The solution was kept stirring during irradiation. At given time intervals, 3 mL of sample was taken out for analysis.

Compared to the blank experiments under the same conditions, it is obvious that the absorption peak of MB, PH, and RhB decreased significantly as time goes by in the presence of

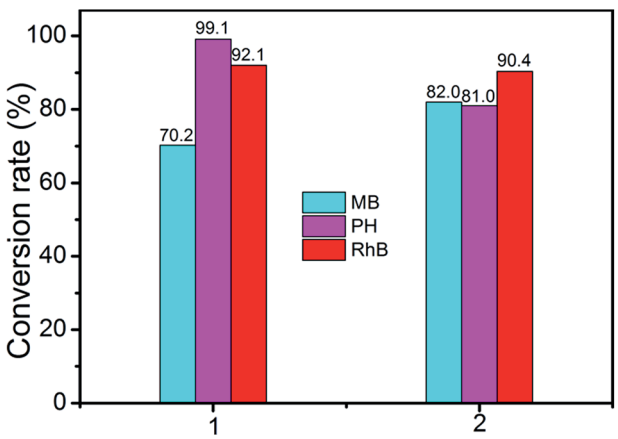

Fig. 10 Conversion rates of the MB, PH and RhB solutions in the presence of compound **1** and **2**.

compounds **1** and **2** (Fig. 9 and Fig. S4†). As shown in Fig. S5,† changes of the concentration of MB, PH, and RhB solution were plotted *versus* irradiation time. The conversions rate of dyes can be expressed as $\alpha = (C_0 - C_t)/C_0$, where C_0 represents the UV-vis intensity of dye at the original reaction time ($t = 0$), C_t is the UV-vis absorption intensity at a certain irradiation time (t). As shown in Fig. 10, the conversion rate of MB is 70.2% for **1** and 82.0% for **2** after irradiation for 3 h. The conversion of PH is 99.1% for **1** and 81% for **2**. The conversion of RhB is 92.1% for **1** and 90.4% for **2**. The results demonstrate that compounds **1** and **2** are good candidates for photocatalytic degradation of MB, PH and RhB.

Conclusions

In conclusion, two new heteropolyoxometalates-directed 3D metal–organic frameworks were synthesized by hydrothermal method. Compounds **1** and **2** both display POM-based pillared-layer 3D frameworks modified by different Cu–tetrazolate motifs. In the structures, compound **1** is a (2,6,6)-connected 3D framework constructed from the 2D networks $\{Cu_5(1,4\text{-ttb})_4(H_2O)_8\}_n$ through connected $CrMo_6$ polyoxoanions with $(3^2.4^2.5^2.6^8.8)(3^4.4^4.5^4.6^3)$ topology. Compound **2** is a (2,3,5)-connected 3D framework constructed from the 2D wave layers $\{Cu_4(1,4\text{-ttb})_4(H_2O)_8\}$ through connected SiW_{12} polyoxoanions with $(4.8^2)_2(4^2.6^4.8^2.10^2)(8)$ topology. The magnetic measurement of compound **1** indicates the presence of dominant antiferromagnetic coupling between magnetic centers. The electrochemistry property of compound **2** is studied. In addition, compounds **1** and **2** display excellent photocatalytic activities for the degradation of several organic dyes. This work provides useful information for the design and construction of multifunctional heteropolyoxometalates-directed 3D metal–organic frameworks with various architectures.

Acknowledgements

Financial support from the National Natural Science Foundation of China (21371078, 21401077) and the open research fund of FJIRSM, CAS (20170034) is gratefully acknowledged.

Notes and references

1 (*a*) W. Salomon, G. Paille, M. Gomez-Mingot, P. Mialane, J. Marrot, C. Roch-Marchal, G. Nocton, C. Mellot-Draznieks, M. Fontecave and A. Dolbecq, *Cryst. Growth Des.*, 2017, **17**, 600; (*b*) S. J. Folkman and R. G. Finke, *ACS Catal.*, 2017, **7**, 7; (*c*) D. Ravelli, S. Protti and M. Fagnoni, *Acc. Chem. Res.*, 2016, **49**, 2232; (*d*) R. Kawahara, R. Osuga, J. N. Kondo, N. Mizuno and S. Uchida, *Dalton Trans.*, 2017, **46**, 3105; (*e*) R. Khoshnavazi, L. Bahrami, F. Havasi and E. Naseri, *RSC Adv.*, 2017, **7**, 11510; (*f*) T. K. N. Luong, I. Govaerts, J. Robben, P. Shestakova and T. N. Parac-Vogt, *Chem. Commun.*, 2017, **53**, 617; (*g*) J. Fielden, J. M. Sumliner, N. N. Han, Y. V. Geletii, X. Xiang, D. G. Musaev, T. Q. Lian and C. L. Hill, *Chem. Sci.*, 2015, **6**, 5531.

2 (*a*) A. Proust, B. Matt, R. Villanneau, G. Guillemot, P. Gouzerh and G. Izzet, *Chem. Soc. Rev.*, 2012, **41**, 7605; (*b*) S. Sadjadi and M. M. Heravi, *Curr. Org. Chem.*, 2016, **20**, 1404; (*c*) J. J. Walsha, A. M. Bondb, R. J. Forstera and T. E. Keyesa, *Coord. Chem. Rev.*, 2016, **306**, 217.

3 (*a*) Y. F. Hui, C. L. Kang, T. Tian, S. Dang, J. Ai, C. Liu, H. R. Tian, Z. M. Sun and C. Y. Gao, *CrystEngComm*, 2017, **19**, 1564; (*b*) M. Song, B. Mu and R. D. Huang, *J. Solid State Chem.*, 2017, **246**, 1; (*c*) X. L. Hu, X. X. Yang, X. Q. He and Z. M. Sun, *Inorg. Chem. Commun.*, 2017, **77**, 35.

4 (*a*) X. Wang, J. Peng, K. Alimajea and Z. Y. Shi, *CrystEngComm*, 2012, **14**, 8509; (*b*) Z. Y. Shi, Z. Y. Zhang, J. Peng, X. Yua and X. Wang, *CrystEngComm*, 2013, **15**, 7199; (*c*) Z. Y. Shi, J. Peng, Z. Y. Zhang, X. Yu, K. Alimaje and X. Wang, *Inorg. Chem. Commun.*, 2013, **33**, 105.

5 T. P. Hu, Y. Q. Zhao, Z. Jagličić, K. Yu, X. P. Wang and D. Sun, *Inorg. Chem.*, 2015, **54**, 7415.

6 (*a*) A. Beni, A. Dei, S. Laschi, M. Rizzitano and L. Sorace, *Chem.– Eur. J.*, 2008, **14**, 1804; (*b*) A. Perloff, *Inorg. Chem.*, 1970, **9**, 2228.

7 X. L. Wang, Z. H. Kang, E. B. Wang and C. W. Hu, *Mater. Lett.*, 2002, **56**, 393.

8 G. M. Sheldrick, *Acta Crystallogr., Sect. A: Found. Crystallogr.*, 2008, **64**, 112.

9 J. T. Shi, K. F. Yue, B. Liu, C. S. Zhou, Y. L. Liu, Z. G. Fang and Y. Y. Wang, *CrystEngComm*, 2014, **16**, 3097.

10 I. D. Brown and D. Altermatt, *Acta Crystallogr., Sect. B: Struct. Sci.*, 1985, **41**, 244.

11 (*a*) X. L. Wang, H. L. Hu, A. X. Tian, H. Y. Lin and J. Li, *Inorg. Chem.*, 2010, **49**, 10299; (*b*) X. L. Wang, J. Li, A. X. Tian, D. Zhao, G. C. Liu and H. Y. Lin, *Cryst. Growth Des.*, 2011, **11**, 3456.

12 X. L. Wang, F. F. Sui, H. Y. Lin, J. W. Zhang and G. C. Liu, *Cryst. Growth Des.*, 2014, **14**, 3438.

13 (*a*) C. H. Gong, X. H. Zeng, C. F. Zhu, J. H. Shu, P. X. Xiao, H. Xu, L. C. Liu, J. Y. Zhang, Q. D. Zeng and J. L. Xie, *RSC Adv.*, 2016, **6**, 106248; (*b*) X. P. Sun, Z. J. Liang, P. T. Ma, R. Ban, M. S. Jiang, D. D. Zhang, J. P. Wang and J. Y. Niu, *Dalton Trans.*, 2015, **44**, 17544; (*c*) P. P. Zhu, L. J. Sun, N. Sheng, J. Q. Sha, G. D. Liu, L. Yu, H. B. Qiu and S. X. Li, *Cryst. Growth Des.*, 2016, **16**, 3215; (*d*) Y. M. Chen, Y. H. Yu, H. Z. Zhang, G. F. Hou, J. S. Gao and P. F. Yan, *CrystEngComm*, 2016, **18**, 6389.

